

Mean DNA Bend Angle and Distribution of DNA Bend Angles in the CAP-DNA Complex in Solution

Achillefs N. Kapanidis¹, Yon W. Ebright¹, Richard D. Ludescher², Shirley Chan³ and Richard H. Ebright^{1*}

¹Howard Hughes Medical Institute, Waksman Institute and Department of Chemistry Rutgers University, Piscataway, NJ 08854, USA

²Department of Food Science Rutgers University, New Brunswick, NJ 08901, USA

³Department of Physics Princeton University Princeton, NJ 08544, USA

In order to define the mean DNA bend angle and distribution of DNA bend angles in the catabolite activator protein (CAP)-DNA complex in solution under standard transcription initiation conditions, we have performed nanosecond time-resolved fluorescence measurements quantifying energy transfer between a probe incorporated at a specific site in CAP, and a complementary probe incorporated at each of five specific sites in DNA. The results indicate that the mean DNA bend angle is $77(\pm 3)^\circ$ – consistent with the mean DNA bend angle observed in crystallographic structures ($80(\pm 12)^\circ$). Lifetime-distribution analysis indicates that the distribution of DNA bend angles is relatively narrow, with <10% of DNA bend angles exceeding 100° . Millisecond time-resolved luminescence measurements using lanthanide-chelate probes provide independent evidence that the upper limit of the distribution of DNA bend angles is $\sim 100^\circ$. The methods used here will permit mutational analysis of CAP-induced DNA bending and the role of CAP-induced DNA bending in transcriptional activation.

© 2001 Academic Press

Keywords: catabolite activator protein (CAP); cAMP receptor protein (CRP); transcriptional activation; protein-induced DNA bending; fluorescence resonance energy transfer

*Corresponding author

Introduction

The *Escherichia coli* catabolite activator protein (CAP; also known as cAMP receptor protein (CRP)) is a sequence-specific DNA-binding protein involved in transcriptional regulation.^{1,2} CAP functions by binding, in the presence of the allosteric effector cAMP, to specific DNA sites in or near promoters and enhancing the ability of RNA polymerase to bind to DNA and initiate transcription. The consensus DNA site for CAP is 22 bp in length and exhibits 2-fold sequence symmetry: 5'-AAATGTGATCTAGATCACATTT-3'.³

Present address: A. N. Kapanidis, Lawrence Berkeley National Laboratory, Berkeley, CA 94720, USA.

Abbreviations used: CAP, catabolite activator protein; CRP, cAMP receptor protein; 1, 5-IAEDANS, 5-[(iodoacetamido-ethyl)-amino]naphthalene-1-sulfonic acid; AEDANS, 5-[(acetamido-ethyl)-amino]naphthalene-1-sulfonic acid; FRET, fluorescence resonance energy transfer; LRET, luminescence resonance energy transfer; FWHM, full width at half maximum.

E-mail address of the corresponding author: ebright@mbcl.rutgers.edu

Crystallographic structures of CAP, of CAP in complex with the consensus DNA site, and of CAP in complex with other DNA sites have been determined (refs. 4–8; J. Liu, G. Parkinson, S. Chen, J. Vojtechovsky, E. Blatter, H. Berman, & R.H.E., unpublished results). CAP is a dimer of two identical subunits, each of which is 209 residues in length and contains a helix-turn-helix DNA-binding motif.⁹ The CAP-DNA complex is 2-fold symmetric: one subunit of CAP interacts with one half of the DNA site; the other subunit of CAP interacts in a 2-fold symmetry-related fashion with the other half of the DNA site. CAP bends DNA sharply in the CAP-DNA complex, yielding a DNA bend angle of $\sim 60^\circ$ to $\sim 90^\circ$ ($80(\pm 12)^\circ$; mean \pm standard deviation for PDB accession numbers 1RUN, 1DB7, 1EHP, 1CGP, 2CGP, and 1BER). The DNA bend is oriented such that the DNA wraps toward and around the sides of the CAP dimer. The DNA bending is distributed approximately equally between the two halves of the DNA site. Within each half-site, DNA bending is localized to two phased kinks: a “primary kink” of $\sim 10^\circ$ to $\sim 50^\circ$ ($41(\pm 24)^\circ$) compressing the DNA major groove between positions 6 and 7, and a

“secondary kink” of 0° to -20° ($-9(\pm 7)^\circ$), compressing the DNA minor groove between positions -1 and 2. The driving force for CAP-induced DNA bending appears to be formation of electrostatic interactions between positively charged residues on the sides of the CAP dimer (Lys26, Lys166, His199, and Lys201; possibly, Lys22 and Lys44) and negatively charged DNA phosphate groups (positions -5 to 2).

It has been proposed that the crystallographic structures may underestimate the DNA bend angle in the CAP-DNA complex, due to crystal lattice constraints and due to the use of relatively short DNA fragments in the crystallographic structures (30-46 bp).^{6,10} Specifically, it has been proposed that the DNA bend angle in the CAP-DNA complex in solution with sufficiently long DNA fragments may be $>100^\circ$, with CAP inducing formation of an additional phased kink in each DNA half-site (“tertiary kink,” compressing the DNA major groove between positions -6 and -4) *via* electrostatic interactions between additional positively charged residues of CAP (His19, His21, Lys22, and Lys44) and additional, more distal, negatively charged DNA phosphates (positions -11 to -5).^{6,10,11}

Electrophoretic mobility shift measurements,¹²⁻¹⁷ electro-optical measurements,¹⁸⁻²⁰ cyclization measurements,²¹⁻²³ and topological measurements²⁴ confirm that CAP bends DNA sharply in solution, and yield estimates of the mean DNA bend angle in the CAP-DNA complex in solution that range from $\sim 70^\circ$ to $\sim 180^\circ$. However, these measurements do not provide direct information regarding the structural organization of the complex but – rather, provide information regarding macroscopic properties of the complex (electrophoretic mobility, ligation rates, DNA topology, or rotational correlation times) that can be related to structural organization only with difficulty – and thus these measurements do not permit direct, accurate quantitation of mean DNA bend angles. In addition, for technical reasons (interference of salt with electrophoresis, electro-optical methods, and ligation), most of these measurements can be performed only under low-salt conditions (0-50 mM monovalent cation), and, to date, none has been performed under standard transcription conditions (40 mM Tris-HCl, pH 8, 100 mM KCl, 10 mM MgCl₂, and 5% glycerol).

Fluorescence resonance energy transfer (FRET) measurements of DNA end-to-end distances in the CAP-DNA complex further confirm that CAP sharply bends DNA in solution and yield an estimate of the mean DNA bend angle of 80° to 100° .²⁵⁻²⁷ FRET measurements of DNA end-to-end distances provide direct information regarding the structural organization of the complex and, in principle, can be performed under standard transcription conditions. However, FRET measurements with conventional fluorescent probes are accurate only for distances less than $\sim 100 \text{ \AA}$.²⁵⁻²⁹ Therefore, accurate FRET measurements of DNA end-to-end distances

in the CAP-DNA complex can be performed only with very short DNA fragments ($\leq 26 \text{ bp}$)²⁵ – i.e., DNA fragments too short to contain the proposed full determinants for CAP-induced DNA bending ($\geq 44 \text{ bp}$),^{11,13} and even too short to contain the full determinants for affinity in the CAP-DNA interaction ($\geq 32 \text{ bp}$)^{13,28} – or with DNA fragments containing multiple non-helical segments.^{26,27}

The absence of an assay permitting direct, accurate quantitation of CAP-induced DNA bending in solution under transcription conditions with sufficiently long, fully helical, DNA fragments has thwarted quantitative comparison of CAP-induced DNA bending in solution to CAP-induced DNA bending in the crystallographic state, has thwarted mutational analysis of CAP-induced DNA bending, and has thwarted assessment of whether and, if so, how CAP-induced DNA bending is involved in transcriptional activation by CAP.

In this work, we use FRET^{29,30} measurements of protein-DNA distances, and luminescence resonance energy transfer (LRET)^{29,31} measurements of DNA end-to-end distances, to quantify the mean DNA bend angle and distribution of DNA bend angles in the CAP-DNA complex in solution under standard transcription conditions. We find that the mean DNA bend angle is $77(\pm 3)^\circ$, a mean DNA bend angle similar to those determined in the crystallographic structures, and that the range of DNA bend angles is $\sim 40^\circ$ to $\sim 100^\circ$. The results set the stage for mutational analysis of CAP-induced DNA bending and the role of CAP-induced DNA bending in transcriptional activation.

Results and Discussion

Mean DNA bend angle in the CAP-DNA complex: standard transcription conditions

In principle, FRET experiments of DNA end-to-end distances can be used to estimate mean DNA bend angles in protein-DNA complexes.^{25-27,32-38} However, in the CAP-DNA complex, in which DNA wraps around the sides of a dimeric protein with a diameter of $\sim 60 \text{ \AA}$, the DNA end-to-end distance for a DNA fragment containing all determinants for interaction and containing no non-helical segments is too long for accurate FRET measurements with conventional fluorescent probes ($>100 \text{ \AA}$; Figures 1 and 2).⁵⁻⁸ Thus, FRET measurements with the CAP-DNA complex using a 32 bp DNA fragment terminally labelled with conventional fluorescent probes yield energy transfer efficiencies of $<2\%$,²⁵ and FRET measurements with the CAP-DNA complex using 40, 42, and 52 bp DNA fragments terminally labelled with conventional fluorescent probes yield energy transfer efficiencies of $<1\%$ (ref. 25; A. Gunasekera & R.H.E., unpublished results).

In this work, as an alternative to FRET measurements of DNA end-to-end distances within the CAP-DNA complex, we have performed FRET measurements of protein-to-DNA distances within

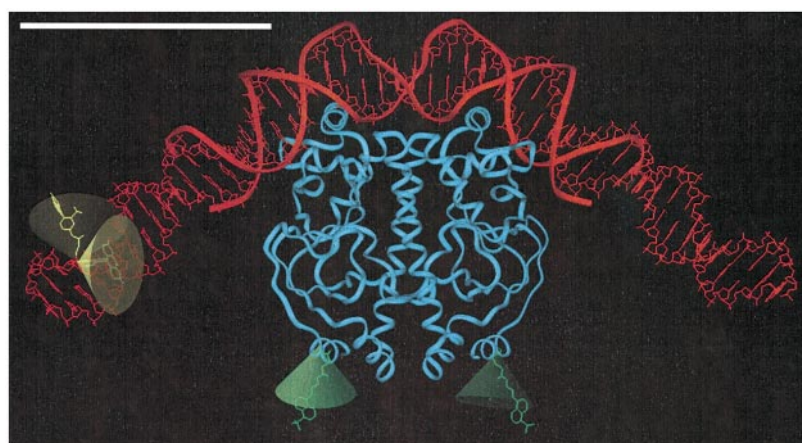


Figure 1. FRET measurements: model for the structure of the CAP^{AEDANS}-ICAP52^{E,-11} complex. CAP is in cyan, DNA is in red, AEDANS (donor) is in green, fluorescein (acceptor; both R_p and S_p diastereomers shown) is in yellow. The green and the yellow cones represent the conformational space sampled by AEDANS and fluorescein as defined in time-resolved anisotropy experiments (see Materials and Methods). The white bar represents 50 Å.

the CAP-DNA complex (Figure 1). This strategy reduces the distances to be measured from >100 Å to 30-70 Å and, correspondingly, increases the energy transfer efficiency to be measured from <2% to 10-40%. We have prepared a CAP derivative having the fluorescent probe 5-[(acetamido-ethyl)-amino]naphthalene-1-sulfonic acid (AEDANS), which can be used as a donor in FRET,³⁹⁻⁴⁰ site-specifically incorporated at position 17 of each CAP protomer (Tables 1 and 2; green in Figures 1 and 2). We have prepared five 52 bp DNA fragments, each containing the consensus DNA site for CAP and the fluorescent probe fluorescein (which can be used as an acceptor to AEDANS in FRET) incorporated at single, defined phosphate groups flanking the DNA site for CAP: i.e., at position -15, -13, -11, -9, or -7 relative to the consensus DNA site for CAP (Tables 1 and 2; yellow in

Figures 1 and 2). For each DNA fragment, we formed the CAP-DNA complex, separated the CAP-DNA complex from unbound CAP, quantified the efficiency of energy transfer (E) using nanosecond time-resolved fluorescence data (Figure 3 and Table 3), and, as a control to verify rapid reorientation of donor and acceptor, and thus to validate interpretation of E solely in terms of donor-acceptor distances, measured steady-state and nanosecond time-resolved anisotropies of probes (Table 2).

To obtain an initial, rough estimate of the DNA bend angle, we compared the measured values of E to expected values of E for DNA bend angles of 10° to 160° – calculating expected values of E from the structural models in Figure 2, considering only the donor incorporated in the CAP subunit proximal to the site of incorporation of acceptor in

Table 1. FRET measurements: spectroscopic properties of labelled complexes

CAP-DNA complex	$\lambda_{\max, \text{exc}}$ (nm)	$\lambda_{\max, \text{em}}$ (nm)	ϵ (M ⁻¹ cm ⁻¹)
CAP ^{AEDANS} -ICAP52	337	502	5,850 ± 100
CAP-ICAP52 ^{E,-15}	499	522	74,000 ± 2000
CAP-ICAP52 ^{E,-13}	493	520	81,000 ± 3000
CAP-ICAP52 ^{E,-11}	492	521	82,000 ± 2000
CAP-ICAP52 ^{E,-9}	492	521	88,000 ± 2000
CAP-ICAP52 ^{E,-7}	492	522	79,000 ± 2000

Table 2. FRET measurements: steady-state and time-resolved fluorescence anisotropies of labelled complexes

CAP-DNA complex	$\langle A \rangle$ (steady-state)	A_0 (time-resolved)	β_G	ϕ_G (ns)	β_L	ϕ_L (ns)	θ_c (deg.)
CAP ^{AEDANS} -ICAP52	0.089 ± 0.03	0.19 ± 0.02	0.11 ± 0.02	25 ± 5	0.08 ± 0.02	1.0 ± 0.5	34
CAP-ICAP52 ^{E,-15}	0.150 ± 0.04						
CAP-ICAP52 ^{E,-13}	0.046 ± 0.02	0.36 ± 0.04	0.06 ± 0.02	12 ± 4	0.30 ± 0.05	0.8 ± 0.4	56
CAP-ICAP52 ^{E,-11}	0.048 ± 0.02						
CAP-ICAP52 ^{E,-9}	0.048 ± 0.02						
CAP-ICAP52 ^{E,-7}	0.047 ± 0.02						

$\langle A \rangle$ is the steady-state fluorescence anisotropy of AEDANS or fluorescein in the CAP-DNA complex; A_0 is the fundamental fluorescence anisotropy of AEDANS or fluorescein in the CAP-DNA complex; β_G and ϕ_G are, respectively, the amplitude and correlation time for global re-orientation of the fluorescent probe, and β_L and ϕ_L are the analogous parameters for local re-orientation of the labelled macromolecule; θ_c is the half-cone angle through which each probe dipole wobbles.

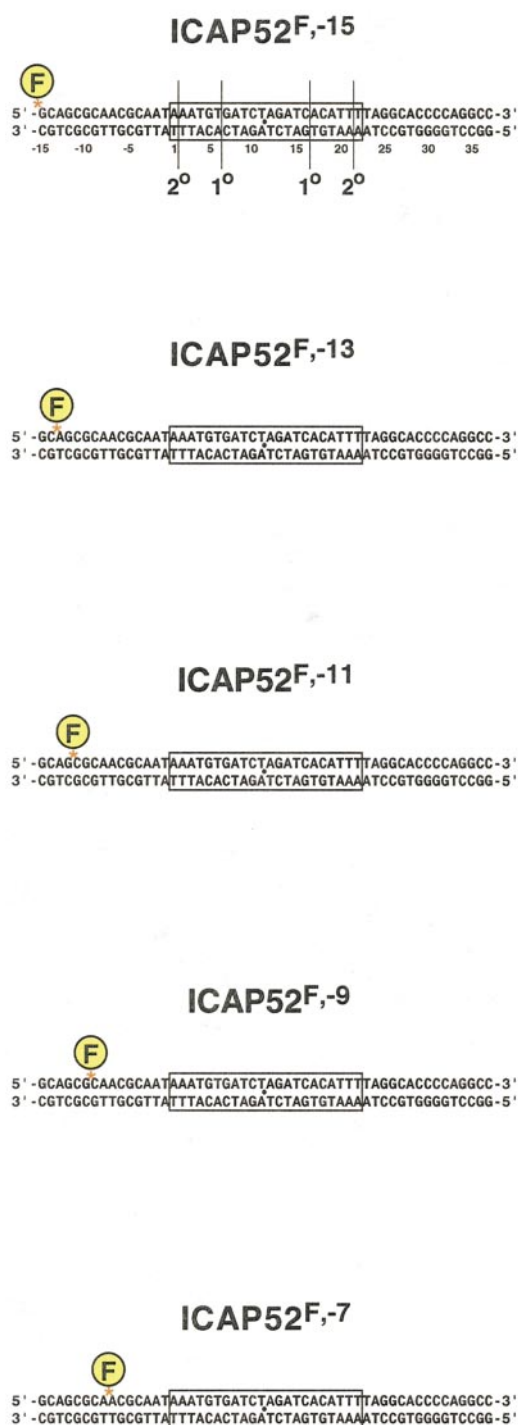


Figure 2. FRET measurements: experimental design. (a) DNA fragments analyzed. Each DNA fragment is 52 bp in length and contains the 22-bp 2-fold symmetric consensus DNA site for CAP (rectangle). Each DNA site also contains fluorescein (circle) incorporated at a single, defined phosphate group (asterisk; phosphate groups 5' to positions -15 , -13 , -11 , -9 , and -7). DNA fragments are named with superscript F indicating the presence of fluorescein, and a superscript number indicating the position at which fluorescein is incorporated. (b) Modelled structures of CAP^{AEDANS}-ICAP52^F complexes with DNA bend angles of 0° , 40° , 50° , 60° , 70° , 80° , 90° , 100° , 110° , and 120° . Sites of incorporation of AEDANS and fluorescein are indicated by green spheres and yellow spheres, respectively. Distances between sites of incorporation of AEDANS and fluorescein vary as a function of DNA bend angle.

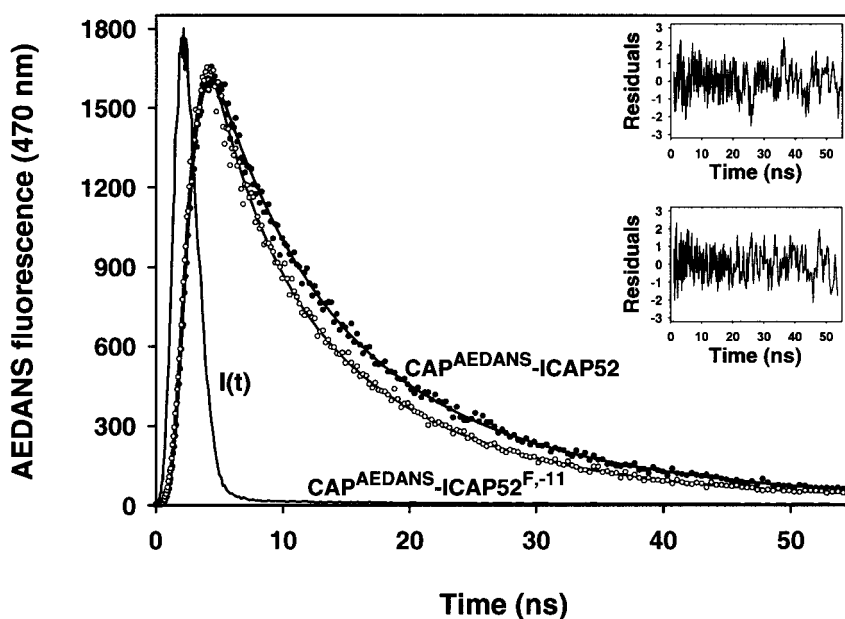


Figure 3. FRET measurements: representative data. AEDANS fluorescence-intensity decays are shown for the CAP^{AEDANS}-ICAP52^{F,-11} complex (open circles) and the CAP^{AEDANS}-ICAP52 complex (donor-only control; filled circles). The instrument response function ($I(t)$), and double-exponential decay fits are shown as continuous lines. Satisfactory χ^2 values (0.91 and 0.98 for CAP^{AEDANS}-ICAP52^{F,-11} and CAP^{AEDANS}-ICAP52, respectively) and random patterns of weighted residuals (inset panels) support the quality of the fitting. The faster fluorescence-intensity decay of the CAP^{AEDANS}-ICAP52^{F,-11} complex *versus* the CAP^{AEDANS}-ICAP52 complex is indicative of energy transfer. From the recovered mean lifetimes (Table 2), the mean energy transfer for the CAP^{AEDANS}-ICAP52^{F,-11} complex is calculated to be 19%.

DNA (which, due to the inverse-sixth-power relationship between distance and E ,^{29,30} is responsible for the majority of E), and modelling probes as discrete points at sites of incorporation (see Materials and Methods). The best fits were obtained with structural models with DNA bend angles of 70°-90° (not shown).

To obtain a more accurate estimate of DNA bend angle, we compared the measured values of E to expected values of E for DNA bend angles of 60°, 70°, 80°, 90°, and 100°, in this case, considering the donors in both CAP subunits, and explicitly accounting for the conformations and dynamics of probes (see Materials and Methods). Within experimental error, all measured values of E were in the

range of expected values of E for DNA bend angles of 70° to 80° (Figure 4, cf. filled circles and heavy line *versus* light lines). We then calculated and plotted root-mean-square differences between measured values of E and expected values of E (rmsd_E ; Figure 4, inset). The minimum of a spline fit of the plot of rmsd_E *versus* DNA bend angle was 77° (Figure 4, inset). The rmsd_E for 77° was 1.3%; for comparison, the rmsd_E for 70° was 3.0%, and the rmsd_E for 80° was 1.8%. We conclude that the mean DNA bend angle in the CAP-DNA complex in solution in standard transcription buffer is 77° with an uncertainty of $\sim \pm 3^\circ$.

The mean DNA bend angle estimated in this work (77(± 3)°) is in excellent agreement with DNA

Table 3. FRET measurements: AEDANS fluorescence lifetimes, E , and R_o

CAP-DNA complex	χ^2	α_1	τ_1 (ns)	α_2	τ_2 (ns)	$\langle \tau \rangle$ (ns)	E (%)	R_o (Å)
CAP ^{AEDANS} -ICAP52	0.99	0.31 ± 0.03	4.5 ± 0.3	0.69 ± 0.03	13.9 ± 0.1	10.9 ± 0.2		
CAP ^{AEDANS} -ICAP52 ^{F,-15}	1.10	0.40 ± 0.02	4.0 ± 0.4	0.60 ± 0.02	12.8 ± 0.2	9.3 ± 0.5	14 ± 2	47.9
CAP ^{AEDANS} -ICAP52 ^{F,-13}	0.99	0.33 ± 0.02	3.5 ± 0.1	0.68 ± 0.02	12.5 ± 0.2	9.6 ± 0.1	13 ± 1	48.5
CAP ^{AEDANS} -ICAP52 ^{F,-11}	0.95	0.41 ± 0.04	3.9 ± 0.1	0.60 ± 0.04	12.4 ± 0.2	8.9 ± 0.2	19 ± 1	48.5
CAP ^{AEDANS} -ICAP52 ^{F,-9}	1.10	0.48 ± 0.01	2.6 ± 0.1	0.52 ± 0.01	12.1 ± 0.3	7.5 ± 0.1	32 ± 2	48.8
CAP ^{AEDANS} -CAP52 ^{F,-7}	1.25	0.52 ± 0.02	3.0 ± 0.1	0.49 ± 0.02	11.9 ± 0.5	7.3 ± 0.2	34 ± 2	48.3

χ^2 is the statistic describing fit of the double-exponential-decay model to the experimental fluorescence-intensity decay; α_1 and α_2 are the amplitudes, and τ_1 and τ_2 are the lifetimes, of the decay components, as described by $F(t) = \Sigma \alpha_i \exp(-t/\tau_i)$; $\langle \tau \rangle$ is the mean lifetime calculated as in equation (2); E is the efficiency of resonance energy transfer from a fluorescent donor to a fluorescent acceptor; R_o is the donor-acceptor distance at which the efficiency of energy transfer equals 50%. Data represent means of at least four fluorescence-intensity-decay measurements per CAP-DNA complex.

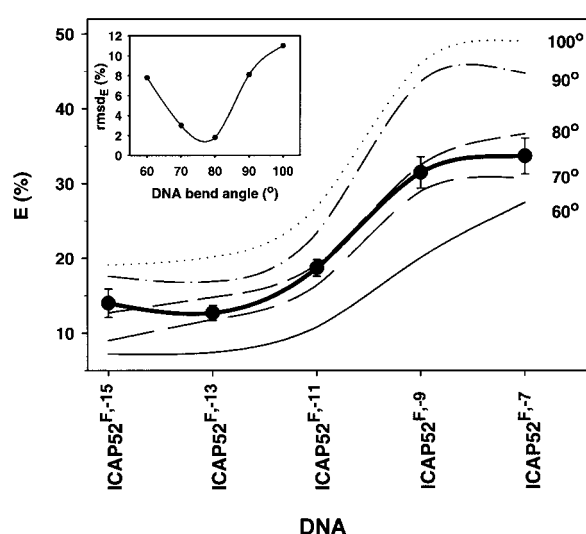


Figure 4. FRET measurements: mean DNA bend angle in the CAP-DNA complex in solution. Main panel, observed values of energy transfer (filled circles and heavy lines) and expected values of energy transfer for modelled DNA bend angles of 60°, 70°, 80°, 90°, and 100° (light lines) are shown for the CAP^{AEDANS}-ICAP52^{F,-15}, CAP^{AEDANS}-ICAP52^{F,-13}, CAP^{AEDANS}-ICAP52^{F,-11}, CAP^{AEDANS}-ICAP52^{F,-9}, and CAP^{AEDANS}-ICAP52^{F,-7} complexes. Inset, root-mean-square differences between observed values of energy transfer and expected values of energy transfer (rmsd_E) plotted as a function of DNA bend angle. The minimum of the plot defines the mean DNA bend angle (77°).

bend angles observed in crystallographic structures of the CAP-DNA complex ($80(\pm 12)^\circ$; mean \pm standard deviation for PDB accession numbers 1RUN, 1DB7, 1EHP, 1CGP, 2CGP, and 1BER⁵⁻⁸) and is at the low end of the range of the DNA bend angles estimated from solution measurements (70° - 180°).¹¹⁻²⁵ The excellent agreement with the crystallographic structures rules out proposals^{6,10} that crystallographic structures underestimate DNA bending due to crystal lattice constraints or due to the use of relatively short DNA fragments.

Mean DNA bend angle in the CAP-DNA complex: buffer-composition effects

We have performed analogous FRET measurements in a divalent-cation-free buffer at each of six NaCl concentrations: 0, 25, 50, 100, 150, and 200 mM (Table 4). The results indicate that the mean DNA bend angle decreases with increasing NaCl concentration, decreasing from $\sim 80^\circ$ at 0 mM NaCl to $\sim 60^\circ$ at 200 mM NaCl. The observation that the mean DNA bend angle decreases with increasing NaCl concentration supports the proposal that electrostatic interactions between positively charged residues on the sides of the CAP dimer and negatively charged DNA phosphate groups, and concomitant counterion release, provide a driving force for CAP-induced DNA bending.^{6,10,11,13,41} The mean DNA bend angle in transcription buffer (77°; Figure 4; Table 4) is somewhat higher than the mean DNA bend angle in divalent-cation-free buffer at comparable monovalent-cation concentrations ($\sim 70^\circ$; Table 4). This observation suggests that divalent cations, specifically Mg^{2+} , may have a specific role in facilitating CAP-induced DNA bending.

We have performed measurements in the buffer used to assay CAP-induced DNA bending in electrophoretic mobility shift experiments: i.e., $0.5 \times \text{TBE}$.^{11,14,42} The mean DNA bend angle in $0.5 \times \text{TBE}$ as measured by FRET was 79° (Table 4). This value is similar to the mean DNA bend angle in transcription buffer as measured by FRET (77°; Figure 4; Table 4), but is very different from DNA bend angle as measured in electrophoretic mobility shift experiments ($\sim 100^\circ$ - $\sim 140^\circ$).¹⁴⁻¹⁷ We attribute this difference to limitations of electrophoretic mobility shift DNA-bending experiments, and of the theoretical framework for relating electrophoretic mobilities to DNA bend angles.

Distribution of DNA bend angles: FRET

To assess the distribution of DNA bend angles in the population of CAP-DNA complexes in

Table 4. FRET measurements: buffer-composition effects

Buffer	Monovalent cation concentration (mM)	Divalent cation concentration (mM)	DNA bend angle ^a (deg)
TBC ^b	120	10	77
DCF ^c	7	0	83
DCF + 25 mM NaCl	32	0	80
DCF + 50 mM NaCl	57	0	73
DCF + 100 mM NaCl	110	0	70
DCF + 150 mM NaCl	160	0	66
DCF + 200 mM NaCl	210	0	62
$0.5 \times \text{TBE}^d$	40	0	79

^a All data are corrected for buffer-composition effects on spectroscopic properties of probes (Q_D , $F_D(\lambda)$, and $\epsilon_A(\lambda)$; equations (11) and (12)).

^b TBC (transcription buffer containing cAMP): 40 mM Tris-HCl (pH 8), 100 mM KCl, 10 mM MgCl_2 , 1 mM dithiothreitol, 5% glycerol, 0.2 mM cAMP.

^c DCF (divalent cation-free buffer): 10 mM Tris-HCl (pH 8), 1 mM dithiothreitol, 5% glycerol, 0.2 mM cAMP.

^d $0.5 \times \text{TBE}$ ($0.5 \times$ Tris-borate-EDTA buffer): 45 mM Tris-borate (pH 8), 0.1 mM EDTA, 0.2 mM cAMP.

solution in transcription buffer, we performed fluorescence-lifetime-distribution analysis.⁴³ Heterogeneity of fluorescence lifetimes in populations of CAP^{AEDANS}-ICAP52^F complexes arises from two sources: (i) differences in DNA bend angles ("DNA-bend-angle heterogeneity"), and (ii) differences associated with probes ("probe heterogeneity"; i.e., the presence of multiple probe conformations, the presence of R_p and S_p acceptor diastereomers, and the presence of two copies of donor per complex (Figures 1 and 2)). We are able to correct in part, but not in full, for probe heterogeneity. Therefore, fluorescence-lifetime-distribution analysis provides an upper limit, not an absolute estimate, of DNA-bend-angle heterogeneity.

The distribution of AEDANS fluorescence lifetimes in the CAP^{AEDANS}-ICAP52^{F,-13} complex (a complex with relatively long distances between probes (Figure 2) and thus relatively less subject to complications arising from probe heterogeneity) was calculated from nanosecond time-resolved fluorescence decays using the exponential series method.⁴⁴⁻⁴⁵ The distribution of AEDANS lifetimes was bimodal, with one peak centered at 12.5 ns (τ_2 ; full width at half maximum (FWHM) of 2.5 ns), and a second peak centered at 3.5 ns (τ_1 ; FWHM of 1.7 ns) (Figure 5(a); see also discrete exponential analysis in Table 3). A histogram representing the corresponding distribution of energy transfer was calculated (Figure 5(b)), using $E = 1 - (\tau_{2,AEDANS+F}/\tau_{2,AEDANS})$, where $\tau_{2,AEDANS+F}$ represents points along the τ_2 lifetime distribution, and $\tau_{2,AEDANS} = 13.9$ ns (Figure 5(a); Table 3, data for CAP^{AEDANS}-ICAP52). Finally, a histogram representing the corresponding distribution of DNA bend angles was calculated (Figure 5(c)), relating each value of E to expected values of E for DNA bend angles of 60°-120° (Figure 4).

The resulting distribution of DNA bend angles exhibited a FWHM of ~65°, with <15% of DNA bend angles in the distribution exhibiting DNA bend angles >100° (Figure 5(c)). Correction, in part, for probe heterogeneity arising from the presence of multiple probe conformations and the presence of R_p and S_p acceptor diastereomers reduced FWHM to 55-60°, with <10% of complexes exhibiting DNA bend angles >100° (not shown). We conclude that the distribution of DNA bend angles in the CAP-DNA complex in solution is relatively narrow, with DNA bend angles substantially higher than those in the crystallographic structures being present in only a small minority of complexes.

Distribution of DNA bend angles: LRET

Whereas FRET measurements of DNA end-to-end distances in the CAP-DNA complex are possible only for short DNA fragments or for DNA fragments with non-helical segments,²⁵⁻²⁷ LRET measurements are possible for relatively long, fully

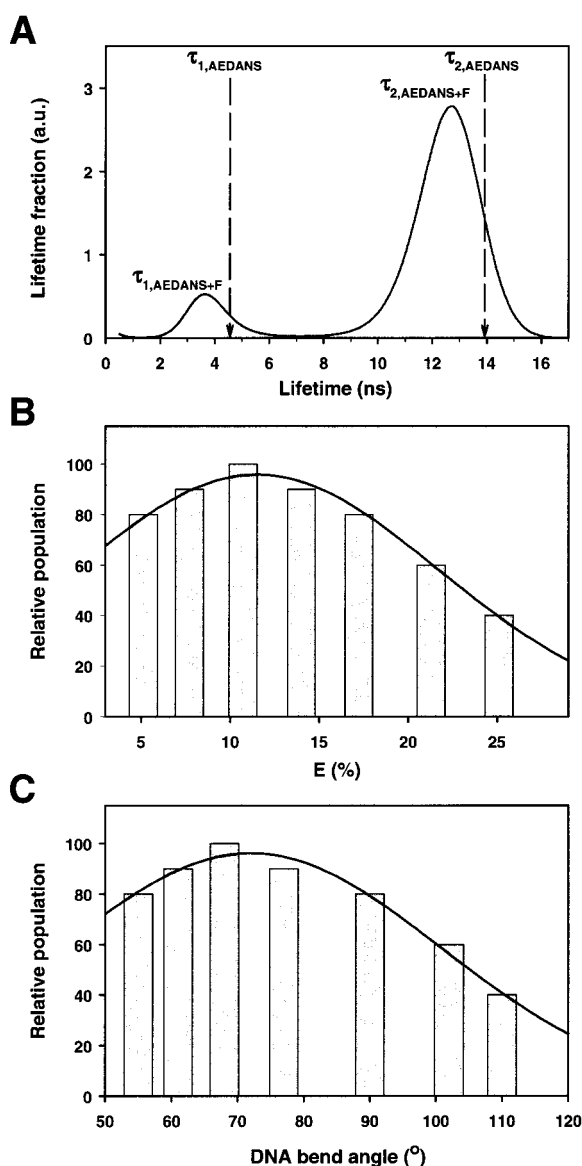


Figure 5. FRET measurements: distribution of DNA bend angles in the CAP-DNA complex in solution. (a) Distribution of AEDANS fluorescence lifetimes in the CAP^{AEDANS}-ICAP52^{F,-13} complex (heavy line). Arrows, mean AEDANS fluorescence lifetimes ($\tau_{1,AEDANS}$ and $\tau_{2,AEDANS}$) for the donor-only control CAP^{AEDANS}-ICAP52 complex. (b) Histogram of the distribution of energy transfer values, E , in the CAP^{AEDANS}-ICAP52^{F,-13} complex. Heavy line, Gaussian distribution fit. (c), Histogram of the maximum distribution of DNA bend angle in the CAP^{AEDANS}-ICAP52^{F,-13} complex. Heavy line, Gaussian distribution fit.

helical, DNA fragments (due to the availability of LRET pairs with $R_0 > 65$ Å, and to the high signal-to-background ratios of LRET detection.^{29,31,46,47} LRET involves energy transfer on time-scales that are long relative to those for protein and nucleic acid dynamics (millisecond time-scale for LRET with Tb(III)-chelate probes^{31,46,47} versus pico- to microsecond time-scale for most protein⁴⁸ and

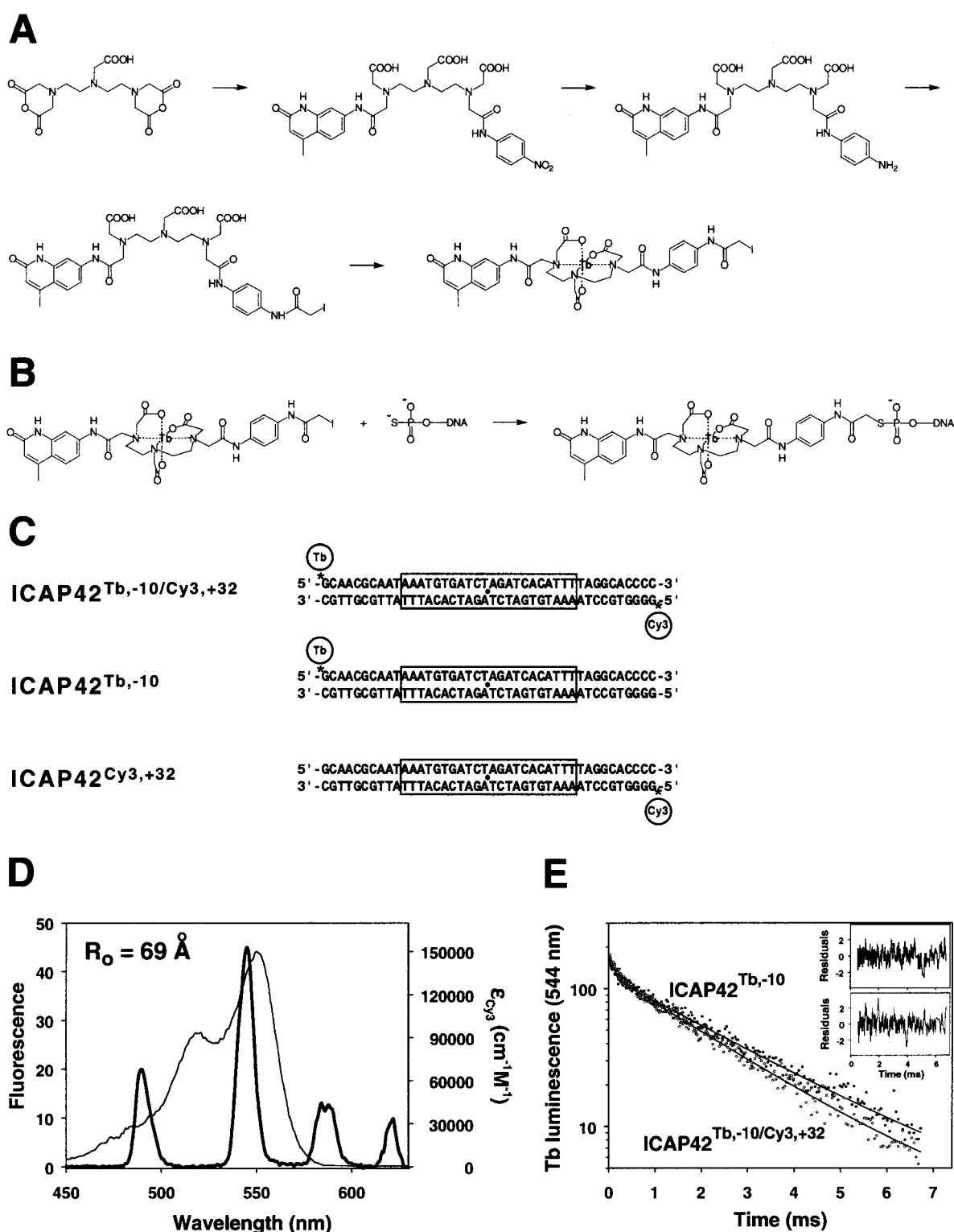


Figure 6. LRET measurements. (a) Synthesis of *N*-(iodoacetyl)-*p*-phenylenediamine-diethylenetriaminepentaacetic acid-carbostyryl-124:Tb(III). (b) Incorporation of *N*-(acetyl)-*p*-phenylenediamine-diethylenetriaminepentaacetic acid-carbostyryl-124:Tb(III) at the 5' end of a 5'-phosphorothioate oligodeoxyribonucleotide. (c) DNA fragments analyzed. Each DNA fragment is 42 bp in length and contains the 22-bp, 2-fold symmetric DNA site for CAP (rectangle). DNA fragment ICAP42^{Tb,-10/Cy3,+32} contains a Tb(III) chelate at one end and Cy3 at the other end. DNA fragment ICAP42^{Tb,-10} contains only the Tb(III) chelate and serves as a donor-only control. DNA fragment ICAP42^{Cy3,+32} contains only Cy3 and serves as an acceptor-only control. (d), Emission spectrum for the CAP-ICAP42^{Cy3,+32} complex (heavy line) and absorbance spectrum for the CAP-ICAP42^{Cy3,+32} complex (light line). R_0 was calculated as 69 Å, using $\kappa^2 = 2/3$, $n = 1.4$, $\epsilon_{\max, \text{Cy3}} = 150,000 \text{ cm}^{-1} \text{ M}^{-1}$, and $Q_{\text{Tb}} = 0.80$ in $^2\text{H}_2\text{O}$.⁷⁶ (e) Representative luminescence-intensity decays for the CAP-ICAP42^{Tb,-10/Cy3,+32} complex (open circles) and the donor-only-control CAP-ICAP42^{Tb,-10} complex (filled circles). The lines are bi-exponential fits; top and bottom insets show residuals. The faster luminescence-intensity decay for the CAP-ICAP42^{Tb,-10/Cy3,+32} complex *versus* the donor-only-control CAP-ICAP42^{Tb,-10} complex indicates the presence of LRET ($E = 15\%$).

nucleic-acid⁴⁹ dynamics). Therefore, LRET measurements define dynamically accessible closest-approach distances between probes, rather than mean distances between probes.^{50,51} We reasoned that LRET measurements of DNA end-to-end distances in the CAP-DNA complex would define the dynamically accessible closest-approach DNA end-to-end distance, and thus would define the dynamically accessible upper limit of the distribution of DNA bend angles.

We prepared a 42 bp DNA fragment containing the DNA site for CAP and having a Tb(III)-chelate probe (*N*-acetyl-*p*-phenylenediamine-diethylenetriaminepentaacetic acid-carbostyryl-124:Tb(III); Figure 6(a) and (b)) incorporated at one end and Cy3 incorporated at the other end (DNA fragment ICAP^{Tb,-10;Cy3,+32}; Figure 6(c)). We then formed the CAP-ICAP^{Tb,-10;Cy3,+32} complex and measured Tb(III) → Cy3 LRET. Following correction for contributions due to diffusion-enhanced intermolecular Tb(III) → Cy3 LRET (see Materials and Methods),^{45,50} we calculated the efficiency of Tb(III) → Cy3 LRET to be 10(±3)% (Table 5). This corresponds to a closest-approach Tb(III)-Cy3 distance of 100(±10) Å, which, in turn, corresponds to a closest-approach DNA end-to-end distance of 110(±15) Å (Table 5). Comparing the observed closest-approach DNA end-to-end distance to the expected DNA end-to-end distances for DNA bend angles of 60°, 70°, 80°, 90°, 100°, 110° and 120° (Figure 2), we estimate the maximum DNA bend angle – the dynamically accessible upper bound of the distribution of DNA bend angles – to be 100°(±20)°. This estimate is in excellent agreement with the upper bound of the distribution of DNA bend angles determined by FRET (~100°; see the preceding section). We conclude that, in the CAP-DNA complex in solution, DNA bend angles substantially higher than those in the crystallographic structures^{5–8} are rare or absent.

Prospect

It has been established that transcriptional activation by CAP at simple CAP-dependent promoters involves protein-protein interaction between CAP and RNA polymerase.² However, it has not been established whether transcriptional activation also involves CAP-induced DNA bending. In principle, CAP-induced DNA bending might be

required to create the appropriate geometry for protein-protein interaction between CAP and RNA polymerase, and/or to create the appropriate DNA conformation for protein-DNA interaction by RNA polymerase. To define possible roles of CAP-induced DNA bending in transcriptional activation, it will be necessary to identify mutants of CAP, or mutants of DNA, specifically defective in CAP-induced DNA bending under standard transcription conditions and to assess their effects on transcriptional activation. The method used here permits, for the first time, identification and characterization of such mutants (A.N.K. and R.H.E., unpublished results).

Materials and Methods

p-Nitroanilino-diethylenetriaminepentaacetic acid-carbostyryl-124

In this and all subsequent synthetic steps, glassware was acid-washed, and aqueous solutions were treated with Chelex-100 (Bio-Rad) to remove any contaminating metals. Diethylenetriaminepentaacetic acid dianhydride (Aldrich, 660 mg, 1.86 mmol) and triethylamine (Aldrich, 1.00 ml, 7.20 mmol) were dissolved in 15 ml of anhydrous dimethylformamide. To the resulting solution, were added over a period of 1.5 hours aliquots of, *p*-nitroaniline (Aldrich, 300 mg, 2.17 mmol, in 5 ml of dimethylformamide) and carbostyryl-124 (Aldrich, 320 mg, 1.86 mmol, in 5 ml of dimethylformamide). Subsequently, 2 ml of deionized water was added, and the reaction mixture was stirred for two hours. The reaction mixture was evaporated to a brown oily solid. The product was purified by flash chromatography (silica gel, 230-400 mesh; NH₄OH/ethanol, 1:4, v/v). Yield 112 mg, 8.5%; MS, *m/e* 670 (M + H)⁺.

p-Phenylenediamine-diethylenetriaminepentaacetic acid-carbostyryl-124

p-Nitroanilino-diethylenetriaminepentaacetic acid-carbostyryl-124 (100 mg, 0.140 mmol) and triethylamine (0.112 ml, 0.806 mmol) were dissolved, with warming, in 5 ml of anhydrous ethanol. To the resulting solution was added 40.0 mg of 10% Pd-charcoal (Aldrich), and the solution was hydrogenated for 12 hours under 1 atm (101,325 Pa) of H₂. The reaction mixture was filtered through Celite (Aldrich) and was evaporated to dryness. The product was purified by flash chromatography (silica gel, 230-400 mesh; NH₄OH/ethanol, 1:4, v/v). Yield: 25.8 mg, 30%.

Table 5. LRET measurements: Tb(III) luminescence lifetimes, E , R_o , and R

CAP-DNA complex	α_1	τ_1 (μ s)	α_2	τ_2 (μ s)	E (%)	E_{intramol} (%)	R_o (Å)	$R_{\text{Tb-Cy3}}$ (Å)	$R_{\text{DNA end-to-end}}$ (Å)
CAP-ICAP42 ^{5b,-10}	0.41	160 ± 30	0.59	2380 ± 30	15 ± 2	10 ± 3	69	100 ± 10	110 ± 15
CAP-ICAP42 ^{Tb,-10/Cy3,+32}	0.43	180 ± 30	0.57	2020 ± 30	15 ± 2	10 ± 3	69	100 ± 10	110 ± 15

α_1 and α_2 are the amplitudes, and τ_1 and τ_2 are the lifetimes, of the decay components, as described by $F(t) = \Sigma \alpha_i \exp(-t/\tau_i)$; E is the sum of intermolecular and intramolecular energy transfer efficiencies; E_{intramol} is the intramolecular energy transfer; $R_{\text{Tb-Cy3}}$ is the closest-approach $R_{\text{Tb(III)-Cy3}}$ distance; $R_{\text{DNA end-to-end}}$ is the closest-approach DNA end-to-end distance.

***N*-(iodoacetyl)-*p*-phenylenediamine-diethylenetriaminepentaacetic acid-carbostyryl-124**

p-Phenylenediamine-diethylenetriaminepentaacetic acid-carbostyryl-124 (12.0 mg, 0.0176 mmol) and triethylamine (0.00234 ml, 0.0170 mmol) were dissolved in 0.5 ml of anhydrous methanol. To the resulting solution was added iodoacetic anhydride (Aldrich, 12.0 mg, 0.034 mmol). The reaction proceeded for 0.5 hour. The resulting suspension was evaporated and triturated, and the solid was collected. Yield 11.5 mg, 77%; MS: *m/e* 795 (M-H).⁻

***N*-(iodoacetyl)-*p*-phenylenediamine-diethylenetriaminepentaacetic acid-carbostyryl-124:Tb(III)**

Reaction mixtures (0.1 ml) contained 6 mM *N*-(iodoacetyl)-*p*-phenylenediamine-diethylenetriaminepentaacetic acid-carbostyryl-124, 6 mM Tb(III)Cl₃ (Aldrich), 20 mM sodium citrate (pH 6), and 50 mM NaCl. Reactions were carried out in the dark and proceeded for 40 minutes at 25 °C.

DNA fragments

Oligodeoxyribonucleotides and phosphorothioate-containing oligodeoxyribonucleotides were prepared as described.⁵² Cy3-labelled oligodeoxyribonucleotides were prepared using Cy3-phosphoramidite (Glen Research), and using dimethylformamido-dG-cyanoethyl phosphoramidite (Glen Research) instead of isobutyrylo-dG-cyanoethyl phosphoramidite (Glen Research). Fluorescein-labelled oligodeoxyribonucleotides were prepared by reaction of 30 mM 5-iodoacetamido-fluorescein (Molecular Probes) and 1 mM phosphorothioate-containing oligodeoxyribonucleotide in 100 μl of 40 mM potassium phosphate (pH 6) and 25% (v/v) dimethylformamide for 18 hours at 37 °C in the dark (pH 7 and six hours at 37 °C for ICAP52^{F,-15}), and were purified by reversed-phase HPLC on a 250 mm × 4 mm LichroCART column (EM Science), using a gradient of 5%-30% (v/v) acetonitrile in 50 mM triethylammonium acetate (pH 7). Tb(III) chelate-labelled oligodeoxyribonucleotides were prepared by reaction of 0.6 mM *N*-(iodoacetyl)-*p*-phenylenediamine-diethylenetriaminepentaacetic acid-carbostyryl-124:Tb(III) and 1 mM phosphorothioate-containing oligodeoxyribonucleotide in 0.5 ml of 20 mM Tris-HCl (pH 8) for four hours at 25 °C in the dark, and were purified by reversed-phase HPLC as described for fluorescein-labelled oligodeoxyribonucleotides. R_p and S_p diastereomers of labelled oligodeoxyribonucleotides⁵³ were not separated.

DNA fragments for FRET (ICAP52, ICAP52^{F,-15}, ICAP52^{F,-13}, ICAP52^{F,-11}, ICAP52^{F,-9}, and ICAP52^{F,-7}; Figure 2) were prepared by annealing oligodeoxyribonucleotides in 10 mM sodium phosphate (pH 7), 500 mM NaCl, and 1 mM EDTA (90 °C for two minutes; cooling from 70 °C to 25 °C over 12 hours). DNA fragments for LRET (Figure 6(c)) were prepared by annealing oligodeoxyribonucleotides in 10 mM Mops-NaOH (pH 7.3) and 200 mM NaCl in ²H₂O (90 °C for one minute; cooling from 70 °C to 4 °C over one hour).

CAP derivatives

Plasmids pAKCRP, pAKCRP[Ser178], and pAKCRP-[Cys17;Ser178] encode CAP, [Ser178]CAP, and

[Cys17;Ser178]CAP, respectively, under the control of bacteriophage T7 gene 10 promoter. Plasmid pAKCRP was constructed by replacement of the *Nde*I-*Hind*III segment of pET21a(+) (Novagen) by the *Nde*I-*Hind*III *crp* segment of plasmid pWNCRP5-N (derivative of plasmid pYZCRP⁵⁴ with cleavage sites for *Nde*I, *Spe*I, and *Xho*I introduced at nucleotides 368, 751, and 940 of *crp* (numbering of nucleotides as in GenBank accession number J01598; A.N.K. & R.H.E., unpublished results). pAKCRP[Ser178] and pAKCRP[Cys17;Ser178] were constructed from pAKCRP by use of site-directed mutagenesis.⁵⁵

For preparation of CAP derivatives, cultures of *Escherichia coli* strain BL21(DE3) (Novagen) transformed with appropriate pAKCRP derivatives were shaken at 37 °C in 1 L LB⁵⁶ containing 200 μg/ml ampicillin until A₆₀₀ = 0.5, isopropyl-β-D-thiogalactoside (IPTG) was added to 1 mM, and cultures were shaken for an additional three hours at 37 °C. Cultures were harvested, and cells were lysed. CAP derivatives were purified by cAMP affinity chromatography, followed by cation-exchange chromatography on Bio-Rex70 (Bio-Rad), followed by gel-filtration chromatography on Biogel-P6DG (Bio-Rad) (methods essentially as described⁵⁷). Concentrations were determined spectrophotometrically ($\epsilon_{\text{CAP protomer}, 278} = 20,000 \text{ M}^{-1}\text{cm}^{-1}$). Yields were ~20 mg, and purities were >99%.

Reaction mixtures (500 μl) for site-specific incorporation of AEDANS at residue 17 of CAP contained 1.5 mM 1,5-IAEDANS (Molecular Probes), 15 μM [Cys17;Ser178]CAP, 0.2 mM cAMP, 20 mM Tris-HCl (pH 8), 200 mM KCl, 0.1 mM EDTA, 0.45 mM dithiothreitol, 5% (v/v) glycerol. Reactions proceeded for five hours at 25 °C in the dark, and were quenched by addition of dithiothreitol to 15 mM and incubation 30 minutes at 25 °C. Products were purified by two rounds of gel-filtration chromatography on NAP-5 (Pharmacia) in transcription buffer containing cAMP (TBC) (40 mM Tris-HCl (pH 8), 100 mM KCl, 10 mM MgCl₂, 1 mM dithiothreitol, 5% glycerol, 0.2 mM cAMP), and were stored in aliquots at -80 °C. Quantification of UV absorbance ($\epsilon_{\text{AEDANS}, 337} = 5850 \text{ M}^{-1}\text{cm}^{-1}$), and quantitation of residual solvent-accessible Cys residues,⁵⁷ establish that ~0.95 mol of AEDANS is incorporated per mol of [Cys17;Ser178]CAP protomer (with the two methods agreeing within 10%). Control experiments establish that, under identical conditions, <0.05 mol of AEDANS is incorporated per mol of [Ser178]CAP protomer, confirming the site-specificity of incorporation. Fluorescence-anisotropy DNA-binding experiments⁵² confirm that CAP^{AEDANS} is fully functional in CAP-DNA complex formation.

CAP-DNA complex formation

Reaction mixtures for CAP-DNA complex formation contained 4 μM CAP derivative and 2 μM ICAP52 derivative in 150 μl of TBC. Following reaction for 20 minutes at 25 °C, complexes were purified from unbound CAP derivative by filtration through a 0.6 ml column of BioRex-70 (Bio-Rad), and were analyzed immediately. Electrophoretic mobility shift experiments¹⁷ indicate that, in the resulting preparations, 96(±1)% of CAP derivative is present as CAP-DNA complexes, and 4(±1)% is present as unbound CAP derivative. The long half-lives of CAP-DNA complexes (>2 hours; data not shown), and the use of concentrations of CAP and DNA much higher than the K_d for CAP-DNA complex

formation (10^{-10} M),³ ensure that no significant dissociation of CAP-DNA complexes occurs during data acquisition.

Time-resolved fluorescence-intensity measurements

Time-resolved fluorescence-intensity measurements were performed using a commercial fluorescence-lifetime instrument (C720, Photon Technology International (PTI)). The excitation source for measurements of AEDANS emission was a pulsed nitrogen laser (GL-3300 (PTI); $\lambda_{\text{exc}} = 337$ nm; pulse width, ~ 500 ps; instrument response function, ~ 1.6 - 1.8 ns FWHM; repetition rate, 10 Hz). The excitation source for measurements of fluorescein emission was a pulsed-nitrogen-laser-pumped dye laser (GL-302 (PTI); $\lambda_{\text{exc}} = 480$ nm; laser dye, coumarin 481 (Exciton)). The laser output was coupled through fiber optics to the sample compartment, and focused in a 100 μl microcuvet (Starna) containing 0.5-1 μM CAP^{AEDANS}-DNA complex in TBC. AEDANS emission at 470 nm and fluorescein emission at 525 nm were monitored using a stroboscopic detector (PTI), after passing through a long-pass filter (KV418, Schott) and a monochromator. Detector signals were amplified and interfaced with a personal computer.

The stroboscopic-optical-boxcar technique⁵⁸ with a random-acquisition mode was used for data acquisition. A digital delay generator (DG535; Stanford Research Systems) triggered by the nitrogen laser set delay times for fluorescence detection. Data were collected for ~ 10 - 15 minutes yielding a signal to noise ratio $>150:1$. (A ratio of 100:1 is equivalent to 10,000 counts at the top-counts channel for time-correlated single photon counting.⁵⁸) Fluorescence-intensity decays were analyzed as exponential decays described as:

$$F(t) = \sum_{i=1}^n \alpha_i \exp(-t/\tau_i) \quad (1)$$

where α_i and τ_i are the amplitude and lifetime, respectively, of each exponential decay. Mean fluorescence lifetimes, $\langle\tau\rangle$, were calculated as:

$$\langle\tau\rangle = \left(\sum_{i=1}^n \alpha_i \tau_i \right) / \left(\sum_{i=1}^n \alpha_i \right) \quad (2)$$

Observed fluorescence decays, $S(t)$, were related to deconvoluted fluorescence-intensity decays, $F(t)$, as:

$$S(t) = \int_0^t I(t')F(t-t') dt' \quad (3)$$

where $I(t')$ is the instrument response function, measured using Ludox silica (Sigma) as scatterer. Data analysis was performed using a non-linear least-squares algorithm and iterative reconvolution.⁵⁹ The criteria for goodness of fit were magnitudes of χ^2 and reduced $\chi^2(\chi^2_{\text{R}})$, randomness of plots of weighted and modified residuals (actual data minus calculated data), and randomness of the autocorrelation function. Color-artifact-shift and analog-background corrections were incorporated in the analysis.⁵⁸ AEDANS fluorescence decays in CAP^{AEDANS}-ICAP52 complexes could not be fit to a single exponential ($\chi^2 > 5$), but could be described well by a sum of two exponentials ($\chi^2 \sim 1.1$; see Figure 3), characterized by a component of ~ 14 ns ($\sim 85\%$ of total intensity) and a component of 4.5 ns ($\sim 15\%$ of total intensity) ($\langle\tau\rangle = 10.9$

ns, where $\langle\tau\rangle$ is the mean fluorescence lifetime). (For reference, fluorescence-intensity decays of 1,5-IAEDANS and other AEDANS-protein conjugates also are bi-exponential or tri-exponential (presumably due to existence of multiple, slowly interconverting conformers (ref. 39, ref. 40, and data not shown)). Fluorescein fluorescence-intensity decays in CAP-ICAP52^{F,-13} (where fluorescein is incorporated at an internal DNA position) also were described well by a sum of two exponentials, with lifetimes of ~ 4.0 ns (90% of total intensity) and ~ 0.80 ns (10% of total intensity) ($\langle\tau\rangle \sim 3.1$ ns; not shown). Fluorescein fluorescence-intensity decays in the CAP-ICAP52^{F,-15} complex (where fluorescein is incorporated at the end of the DNA fragment) exhibited substantial quenching ($\langle\tau\rangle \sim 1$ ns; not shown).

AEDANS fluorescence-intensity decays also were used to recover lifetime distributions,⁴³ using the exponential-series method,^{44,45} which involves fitting fluorescence decays to a series of exponential functions with fixed log-space lifetimes using goodness-of-fit criteria similar to single or multiple-lifetime fitting. Deconvolution of lifetime-distribution components was performed using the additive character of the variance of the components that contribute to the width of lifetime distributions.

Time-resolved luminescence intensity measurements

Time-resolved luminescence-intensity measurements were performed using a commercial phosphorescence/luminescence instrument (QM-2, PTI). The excitation source was a pulsed xenon flashlamp (R-914T (PTI); instrument response function, 80 μs FWHM; repetition rate, 50 Hz), and the detector was a gated photomultiplier tube (PTI). Samples (50 μl) of 0.2 μM CAP-DNA complexes (formed as described above, but omitting the BioRex-70-filtration step), 25 mM Mops-NaOH (pH 7.3) and 200 mM NaCl in $^2\text{H}_2\text{O}$ were excited at 328 nm, and emission was detected at 545 nm. Data were collected for 10-15 minutes (300 channels per decay), and background associated with the gated detector was subtracted. No polarizers were used, since Tb(III)-chelate luminescence is isotropic, and the Cy3 dipole is completely depolarized on the millisecond time-scale. Tb(III)-chelate luminescence-intensity decays were analyzed as described in the previous section. Tb(III)-chelate luminescence-intensity decays in CAP-DNA complexes could not be fit to a single exponential, but could be described well by a sum of two exponentials, characterized by a component of 2380 μs (96% of total intensity) and a component of 160 μs (4% of total intensity) (Figure 6(e)). The 2380 μs lifetime component, typical for Tb(III) chelates in $^2\text{H}_2\text{O}$, participates in energy transfer and was used for LRET measurements (cf. refs. 31, 46).

Steady-state fluorescence anisotropy measurements

Steady-state fluorescence anisotropy measurements were performed using a commercial fluorescence instrument (QM-1, PTI) equipped with T-format Glan-Thompson polarizers (PTI). Steady-state fluorescence anisotropy (A) was measured using:

$$A = (I_{\text{VV}} - GI_{\text{VH}})/(I_{\text{VV}} + 2GI_{\text{VH}}) \quad (4)$$

where I_{VV} and I_{VH} are fluorescence intensities with the excitation polarizer at the vertical position and the emission polarizer at, respectively, the vertical position and the horizontal position, and G is the grating correction

factor.⁶⁰ For AEDANS, anisotropy was measured using 0.5 μM CAP^{AEDANS}-ICAP52 in TBC (excitation wavelength, 340 nm; emission wavelength, 470 nm). For fluorescein, anisotropy was measured using 0.1 μM CAP-ICAP52^F in TBC (excitation wavelength, 480 nm; emission wavelength, 520 nm). Measured steady-state fluorescence anisotropies for AEDANS in CAP^{AEDANS}-ICAP52 complexes, and for fluorescein in CAP-ICAP52^F complexes were low compared to the fundamental anisotropies of the free probes (0.089 *versus* 0.180 (Table 2; ref. 61), and 0.046-0.150 *versus* 0.4 (Table 2; ref. 60)), indicating rapid reorientation of probes during the timescales of the probe lifetimes.

Time-resolved fluorescence anisotropy measurements

Time-resolved fluorescence anisotropy measurements were performed using the instrument used for the time-resolved fluorescence-intensity measurements, with the addition of L-format Glan-Thompson polarizers (PTI) after the excitation monochromator and before the emission monochromator. The excitation polarizer was set to the vertical position, and the emission polarizer was switched between vertical (VV) and horizontal (VH) position at two minute intervals.

Analysis of anisotropy decays included the following steps:⁶² (i) simultaneous analysis of the "raw" decays, I_{VV} and I_{VH} ; (ii) deconvolution of the recovered amplitudes and lifetimes to obtain deconvoluted decays, I_{VV} and I_{VH} ; (iii) calculation of the deconvoluted difference function, $D(t)$, and sum function, $S(t)$; and (iv) calculation of anisotropy decay, $A(t)$, using:

$$A(t) = D(t)/S(t) \quad (5)$$

$$D(t) = I_{VV} - GI_{VH} \quad (6)$$

$$S(t) = I_{VV} + 2GI_{VH} \quad (7)$$

Anisotropy decays were fitted to the following equation:⁴⁰

$$A(t) = \beta_L \exp(-t/\phi_L) + \beta_G \exp(-t/\phi_G) \quad (8)$$

where β_L and ϕ_L are, respectively, the amplitude and correlation time for local re-orientation of the fluorescent probe, and β_G and ϕ_G are the analogous parameters for global re-orientation of the labelled macromolecule.⁴⁰ The sum of β_L and β_G equals the fundamental anisotropy, A_0 , for the wavelengths used (Table 2). Results for AEDANS in the CAP^{AEDANS}-ICAP52 complex revealed both local and a global reorientation of the probe, with the local component accounting for ~40% of anisotropy decay (Table 2). The correlation time for the local component (~0.8 ns) is short compared to the mean AEDANS excited-state lifetime in the CAP^{AEDANS}-ICAP52 complex (10.9 ns; Table 3), indicating that the probe reorients rapidly during the excited-state lifetime, and thus justifying the assumption $\kappa^2 = 2/3$ used in calculation of R_0 . The results for fluorescein in the CAP-ICAP52^F-¹³ complex also revealed both local and global reorientation of the probe, with the local component accounting for ~80% of the anisotropy decay (Table 2), indicating rotational freedom of the probe. Anisotropy parameters were also used to calculate the depolarization factors for each probe, $\langle d_x \rangle$, and the half-cone angle, θ_c , through which each probe dipole wobbles:⁶³

$$\langle d_x \rangle = (\beta_G/A_0)^{1/2} = \cos \theta_c (1 + \cos \theta_c)/2 \quad (9)$$

The values obtained for AEDANS and fluorescein in CAP^{AEDANS}-ICAP52^F complexes were $\langle d_{x,AEDANS} \rangle = 0.76$ with $\theta_{c,AEDANS} = 34^\circ$, and $\langle d_{x,F} \rangle = 0.43$ with $\theta_{c,F} = 56^\circ$ (Table 2; see Figure 1 for cone representation). These values confirm unrestricted local motion of probes and absence of specific probe-macromolecule interactions, further justifying the assumption $\kappa^2 = 2/3$ used in calculation of R_0 .

Fluorescence resonance energy transfer (FRET)

FRET has been extensively used as a "molecular ruler" to measure distances of 10-80 Å between specific sites within macromolecules.^{29,30} For a system containing a fluorescent donor and a fluorescent acceptor, the average donor-acceptor distance, R (in Å), can be calculated from the efficiency of donor \rightarrow acceptor energy transfer, using:

$$E = R_0^6 / (R_0^6 + R^6) \quad (10)$$

where E is the average efficiency of energy transfer, and R_0 is the donor-acceptor distance at which the efficiency of energy transfer equals 50%. R_0 is a function of the spectroscopic properties of donor and acceptor, the relative orientations of donor and acceptor transition dipoles, and the physical properties of the medium:

$$R_0 = 0.211 \times 10^{-5} (n^{-4} Q_D \kappa^2 J)^{1/6} \quad (11)$$

where n is the refractive index of the medium (1.4 for dilute protein solutions),⁴⁰ Q_D is the donor quantum yield in the absence of acceptor (0.39 for AEDANS in the CAP^{AEDANS}-ICAP52 complex in TBC; measured using quinine sulfate in 0.05 M H₂SO₄ as standard ($Q_{QS} = 0.51$)⁴⁰), κ^2 is the orientation factor relating the donor emission dipole and acceptor excitation dipole (approximated as 2/3 for the AEDANS-fluorescein pair in CAP^{AEDANS}-ICAP52^F complexes; see preceding section and below), and J is the spectral overlap integral of the donor emission spectrum and the acceptor excitation spectrum:

$$J = (\int F_D(\lambda) \epsilon_A(\lambda) \lambda^4 d\lambda) / (\int F_D(\lambda) d\lambda) \quad (12)$$

where $F_D(\lambda)$ is the normalized corrected emission spectrum of donor, $\epsilon_A(\lambda)$ is the molar extinction coefficient of acceptor, and λ is the wavelength.

For the CAP^{AEDANS}-ICAP52^F complexes analyzed, R_0 in TBC was determined to be 47.9-48.8 Å (Table 3), a range of R_0 typical for the AEDANS-fluorescein pair.^{39,40} An upper bound on the uncertainty in R_0 arising from uncertainty in the approximation $\kappa^2 = 2/3$ can be estimated from depolarization factors, $\langle d_x \rangle$, obtained from time-resolved fluorescence-anisotropy measurements⁶⁴ (Table 2; see the preceding section). The estimated upper bound on the uncertainty in R_0 is $\pm 15\%$ (41.7-58.8 Å). The actual uncertainty in R_0 will be substantially less than $\pm 15\%$, since uncertainty in the approximation $\kappa^2 = 2/3$ is reduced by three circumstances not addressed by depolarization factors: (i) AEDANS emission exhibits mixed polarization,⁶⁵ (ii) CAP^{AEDANS}-ICAP52^F complexes contain two copies of AEDANS with unsynchronized rotational reorientation (one per CAP subunit), and (iii) populations of CAP^{AEDANS}-ICAP52^F complexes contain 50% R_p diastereomeric fluorescein

and 50% S_p diastereomeric fluorescein (see Materials and Methods, DNA fragments).

The mean efficiency of energy transfer, E , was calculated using:⁴⁰

$$E = 1 - (\langle\tau_{DA}\rangle / \langle\tau_D\rangle) \quad (13)$$

where $\langle\tau_D\rangle$ is the mean donor lifetime in the absence of acceptor, and $\langle\tau_{DA}\rangle$ is the average donor lifetime in the presence of acceptor (average lifetimes calculated as in equation (2)).

Luminescence resonance energy transfer (LRET)

LRET was determined essentially as for FRET. Due to the long excited-state lifetime of the Tb(III)-chelate probe, a significant component of LRET (~30%) results from diffusion-enhanced intermolecular energy transfer. Control experiments were performed at a series of concentrations of CAP-ICAP42^{Tb,-10/Cy3,+32} complexes (20, 30, 50, 80, and 200 μ M) to quantify the diffusion-enhanced intermolecular component of LRET, allowing calculation of intramolecular energy transfer⁴⁷ by subtraction.

Molecular modelling and molecular dynamics

Atomic coordinates for 52 bp DNA fragments with DNA bend angles ranging from 0° to 160°, in steps of 10°, were generated using the program DNA_FIT_MAN.⁴¹ For DNA fragments with DNA bend angles of 10°, 20°, 30°, 40°, 50°, 60°, 70°, and 80°, rolls of, respectively, 5°, 10°, 15°, 20°, 25°, 30°, 35°, and 40°, were introduced between positions 6 and 7 of each DNA half-site ("primary kink"; major groove compressed; see Introduction). For DNA fragments with DNA bend angles of 90°, 100°, and 110°, rolls of 40° were introduced between positions 6 and 7 of each DNA half-site, and rolls of, respectively, -5°, -10°, and -15°, were introduced between positions 1 and 2 of each DNA half-site ("secondary kink"; minor groove compressed; see Introduction). For DNA fragments with DNA bend angles of 120°, 130°, 140°, 150°, and 160°, rolls of 40° were introduced between positions 6 and 7 of each DNA half-site, rolls of, respectively, -15°, -15°, -20°, -20° and -20°, were introduced between positions 1 and 2 of each DNA half-site, and rolls of, respectively, 5°, 10°, 10°, 15°, and 20° were introduced between positions -5 and -4 of each DNA half-site ("tertiary kink"; major groove compressed; see Introduction). (Overall DNA bend angles were defined as the sums of absolute values of introduced roll angles.) Modelled bent DNA fragments were superimposed on the DNA fragment in the crystallographic structure of the CAP-DNA complex,⁵ using all non-hydrogen atoms for positions 7 to 16 of the DNA site for CAP for superimposition (Figure 2(b)).

Probes and linkers were modelled in Insight II (MSI), and minimized in Discover (MSI) (see Figure 1). For each modelled DNA fragment, nine sets of atomic coordinates were generated: i.e., atomic coordinates for DNA fragments with probe at -15, probe at -13 in the R_p configuration, probe at -13 in the S_p configuration, probe at -11 in the R_p configuration, probe at -11 in the S_p configuration, probe at -9 in the R_p configuration, probe at -9 in the S_p configuration, probe at -7 in the R_p configuration, and probe at -7 in the S_p configuration. (The chemistry for preparation of DNA fragments with fluorescein incorporated at internal positions results in a 1:1 distribution of R_p and S_p derivatives.⁴⁷)

For each modelled CAP^{AEDANS}-ICAP52^F complex with a DNA bend angle of 60°-100°, molecular-dynamics simulations^{66,67} were performed to define the ensemble of probe and linker configurations, and thus the ensemble of donor-acceptor distances and expected values of E . Molecular-dynamics simulations were performed *in vacuo* using a dielectric constant of 1 (to simulate solvent-screening effects).⁶⁸ Counterions (CVFF Na⁺) were added 2.5 Å from DNA-phosphate oxygen atoms. Potentials and partial charges for all atoms of CAP^{AEDANS} and of positions -15 to -6 of ICAP52^F were assigned in Discover. The RATTLE algorithm⁶⁹ was used to constrain covalent bond lengths. Positions of atoms of CAP^{AEDANS} other than of atoms AEDANS and linker (defined as atoms distal to Cys17 C^z), and positions of atoms of ICAP52^F other than atoms of fluorescein and linker (defined as atoms distal to the phosphorothioate phosphorus atoms), were held constant. Energy minimization was performed in two stages to obtain starting coordinates: first, for counterions; and second, for probes and linkers (600 steps per stage, 1.0 convergence limit). Molecular-dynamics simulation then was performed, with an equilibration stage of 10 ps in 2 fs timesteps, and a data-collection stage of 1000 ps in 2 fs timesteps. The molecular-dynamics simulation employed a constant-temperature, constant-volume ensemble with an initial temperature of 298° K, initial velocities from a Gaussian distribution of velocities (generated using random-number seeds), the CVFF force-field⁷⁰⁻⁷² with Verlet velocity integrator,⁷³ and calculation of non-bonding interactions using the cell-multipole method⁷⁴ with all atom pairs included. At each 5 ps interval in the 1000 ps data-collection phase of the molecular-dynamics simulation, the conformation was sampled, the AEDANS-fluorescein distances (defined as the distances between the centers of symmetry of the fused aromatic ring systems of the probes⁷⁵) for AEDANS in the proximal CAP subunit and AEDANS in the distal CAP subunit were measured, and the corresponding conformation-specific value of E , E_{conf} was calculated as:

$$E_{conf} = [R_0^6 / (R_0^6 + R_1^6) + R_0^6 / (R_0^6 + R_2^6)] / 2 \quad (15)$$

where R_1 is the AEDANS-fluorescein distance for AEDANS in the proximal CAP subunit, and R_2 is the AEDANS-fluorescein distance for AEDANS in the distal CAP subunit.

For each modelled DNA bend angle of the CAP^{AEDANS}-ICAP52^{F,-13}, CAP^{AEDANS}-ICAP52^{F,-11}, CAP^{AEDANS}-ICAP52^{F,-9}, and CAP^{AEDANS}-ICAP52^{F,-7} complexes, the expected value of E , E_{exp} , was calculated as:

$$E_{exp} = \left(\sum_{i=1}^{200} E_{conf,Rp} + \sum_{i=1}^{200} E_{conf,Sp} \right) / 400 \quad (16)$$

where $E_{conf,Rp}$ is E_{conf} for R_p diastereomeric fluorescein, and $E_{conf,Sp}$ is E_{conf} for S_p diastereomeric fluorescein. For each modelled DNA bend angle of the CAP^{AEDANS}-ICAP52^{F,-15} complexes, E_{exp} was calculated as:

$$E_{exp} = \left(\sum_{i=1}^{200} E_{conf} \right) / 200$$

In addition to the molecular-dynamics approach described above, three alternative approaches were used to calculate E_{exp} : (i) calculation based on distances between sites of incorporation of probes on CAP and

DNA, neglecting AEDANS in the distal CAP subunit (which, due to the inverse-sixth-power relationship between distance and E , makes only a small contribution to E), (ii) calculation based on distances between sites of incorporation of probes on CAP; and (iii) calculation based on distances between probes modelled with fully extended linkers (data not shown). Like the molecular-dynamics approach, these alternative approaches yield values of E_{exp} that, in conjunction with measured values of E (Table 3 and Figure 3), indicate that the mean DNA bend angle is between 70° and 80° (77° ($\text{rmsd}_E = 1.8\%$) for molecular-dynamics approach; 80° ($\text{rmsd}_E = 7.9\%$) for alternative approach (i); 73° ($\text{rmsd}_E = 3.2\%$) for alternative approach (ii); and 75° ($\text{rmsd}_E = 6.2\%$), for alternative approach (iii)).

Acknowledgements

We thank Y. Ma for development of procedures for site-specific incorporation of AEDANS into CAP; R. Austin for preliminary experiments and discussions; Y. Jia and R. Hochstrasser for access to the Regional Laser and Biotechnology Laboratory, Philadelphia, PA, where pilot experiments were performed; and J. Beechem, H. Berman, S. Chen, E. Gratton, W. Olson, and A. Srinivasan for discussions. A.N.K. was partially supported by the State Scholarship Foundation, Athens, Greece. This work was supported by NIH grant GM41376 and a Howard Hughes Medical Institute Investigatorship to R.H.E.

References

- Kolb, A., Busby, S., Buc, H., Garges, S. & Adhya, S. (1993). Transcriptional regulation by cAMP and its receptor protein. *Ann. Rev. Biochem.* **62**, 749-795.
- Busby, S. & Ebright, R. H. (1999). Transcription activation by catabolite activator protein (CAP). *J. Mol. Biol.* **293**, 199-213.
- Ebright, R. H., Ebright, Y. & Gunasekera, A. (1989). Consensus DNA site for the *Escherichia coli* catabolite gene activator protein (CAP): CAP exhibits a 450-fold higher affinity for the consensus DNA site than for the *E. coli* lac DNA site. *Nucl. Acids Res.* **17**, 10295-10305.
- Weber, I. T. & Steitz, T. A. (1987). Structure of a complex of catabolite gene activator protein and cAMP refined to 2.5 Å resolution. *J. Mol. Biol.* **198**, 311-326.
- Parkinson, G., Wilson, C., Gunasekera, A., Ebright, Y., Ebright, R. H. & Berman, H. (1996). Structure of the CAP-DNA complex at 2.5 Å resolution: a complete picture of the protein-DNA interface. *J. Mol. Biol.* **260**, 395-408.
- Schultz, S. C., Shields, G. C. & Steitz, T. A. (1991). Crystal structure of a CAP-DNA complex: the DNA is bent by 90° . *Science*, **253**, 1001-1007.
- Parkinson, G., Gunasekera, A., Voytechovsky, J., Zhang, X., Kunkel, T. A., Berman, H. & Ebright, R. H. (1996). Aromatic hydrogen bond in sequence-specific protein DNA recognition. *Nature Str. Biol.* **3**, 837-841.
- Passner, J. M. & Steitz, T. A. (1997). The structure of a CAP-DNA complex having two cAMP molecules bound to each other. *Proc. Natl Acad. Sci. USA*, **94**, 2843-2847.
- Brennan, R. G. & Matthews, B. W. (1989). The helix-turn-helix DNA binding motif. *J. Biol. Chem.* **264**, 1903-1906.
- Crothers, D. M. & Steitz, T. A. (1992). Transcriptional activation by *Escherichia coli* CAP protein. In *Transcriptional regulation* (McKnight, S. L. & Yamamoto, K. R., eds), 501-534. CSH Press, Cold Spring Harbor.
- Gartenberg, M. R. & Crothers, D. M. (1988). DNA sequence determinants of CAP-induced bending and protein binding affinity. *Nature*, **333**, 824-829.
- Wu, H. M. & Crothers, D. M. (1984). The locus of sequence-directed and protein-induced DNA bending. *Nature*, **308**, 509-513.
- Liu-Johnson, H.-N., Gartenberg, M. R. & Crothers, D. M. (1986). The DNA binding domain and bending angle of *E. coli* CAP protein. *Cell*, **47**, 995-1005.
- Thompson, J. F. & Landy, A. (1988). Empirical estimation of protein-induced DNA bending angles: applications to λ site-specific recombination complexes. *Nucl. Acids Res.* **16**, 9687-9705.
- Zinkel, S. S. & Crothers, D. M. (1990). Comparative gel electrophoresis measurement of the DNA bend angle induced by the catabolite activator protein. *Biopolymers*, **29**, 29-38.
- Zinkel, S. S. & Crothers, D. M. (1991). Catabolite activator protein-induced DNA bending in transcription initiation. *J. Mol. Biol.* **219**, 201-215.
- Zhou, Y., Zhang, X. & Ebright, R. H. (1993). Identification of the activating region of catabolite gene activator protein (CAP): isolation and characterization of mutants of CAP specifically defective in transcription activation. *Proc. Natl Acad. Sci. USA*, **90**, 6081-6085.
- Porschke, D., Hillen, W. & Takahashi, M. (1984). The change of DNA structure by specific binding of the cAMP receptor protein from rotation diffusion and dichroism measurements. *EMBO J.* **3**, 2873-2878.
- Antosiewicz, J. & Porschke, D. (1988). Turn of promoter DNA by cAMP receptor protein characterized by bead model simulation of rotational diffusion. *J. Biomol. Struct. Dynam.* **5**, 819-837.
- Meyer-Almes, F.-J. & Porschke, D. (1997). The cyclic AMP receptor promoter DNA complex: a comparison of crystal and solution structure by quantitative molecular electrooptics. *J. Mol. Biol.* **269**, 842-850.
- Kotlarz, D., Fritsch, A. & Buc, H. (1986). Variations of intramolecular ligation rates allow the detection of protein-induced bends in DNA. *EMBO J.* **5**, 799-803.
- Kahn, J. D. & Crothers, D. M. (1992). Protein-induced bending and DNA cyclization. *Proc. Natl Acad. Sci. USA*, **89**, 6343-6347.
- Kahn, J. D. & Crothers, D. M. (1998). Measurement of the DNA bend angle induced by the catabolite activator protein using Monte Carlo simulation of cyclization kinetics. *J. Mol. Biol.* **276**, 287-309.
- Lutter, L. C., Halvorson, H. R. & Calladine, C. R. (1996). Topological measurement of protein-induced DNA bend angles. *J. Mol. Biol.* **261**, 620-633.
- Heyduk, T. & Lee, J. C. (1992). Solution studies of the structure of bent DNA in the cAMP receptor protein-lac DNA complex. *Biochemistry*, **31**, 5165-5171.
- Stühmeier, F., Hillisch, A., Clegg, R. M. & Diekmann, S. (2000). Fluorescence energy transfer analysis of DNA structures containing several bulges and their interaction with CAP. *J. Mol. Biol.* **302**, 1081-1100.

27. Hillisch, A., Lorenz, M. & Diekmann, S. (2001). Recent advances in FRET: distance determination in protein-DNA complexes. *Curr. Opin. Struct. Biol.* **11**, 201-207.
28. Gunasekera, A., Ebright, Y. W. & Ebright, R. H. (1992). DNA sequence determinants for binding of the *Escherichia coli* catabolite gene activator protein. *J. Biol. Chem.* **267**, 14713-14720.
29. Selvin, P. R. (2000). The renaissance of fluorescence resonance energy transfer. *Nature Struct Biol.* **7**, 730-734.
30. Lilley, D. M. & Wilson, T. J. (2000). Fluorescence resonance energy transfer as a structural tool for nucleic acids. *Curr. Opin. Chem. Biol.* **4**, 507-517.
31. Selvin, P. R., Rana, T. M. & Hearst, J. E. (1994). Luminescence resonance energy transfer. *J. Am. Chem. Soc.* **116**, 6029-6030.
32. Parkhurst, K. M., Brenowitz, M. & Parkhurst, L. J. (1996). Simultaneous binding and bending of promoter DNA by the TATA binding protein: real-time kinetic measurements. *Biochemistry*, **35**, 7459-7465.
33. Ozaki, H., Iwase, N., Sawai, H., Kodama, T. & Kyogoku, Y. (1997). Detection of DNA bending in a DNA-PAP1 protein complex by fluorescence resonance energy transfer. *Biochem. Biophys. Res. Commun.* **231**, 553-556.
34. Jamieson, E. R., Jacobson, M. P., Barnes, C. M., Chow, C. S. & Lippard, S. J. (1999). Structural and kinetic studies of a cisplatin-modified DNA icosamer binding to HMG1 domain B. *J. Biol. Chem.* **274**, 12346-12354.
35. Lorenz, M., Hillisch, A., Payet, D., Buttinelli, M., Travers, A. & Diekmann, S. (1999). DNA bending induced by high mobility group proteins studied by fluorescence resonance energy transfer. *Biochemistry*, **38**, 12150-12158.
36. Lorenz, M., Hillisch, A., Goodman, S. D. & Diekmann, S. (1999). Global structure similarities of intact and nicked DNA complexed with IHF measured in solution by fluorescence resonance energy transfer. *Nucl. Acids Res.* **27**, 4619-4625.
37. Wu, J., Parkhurst, K. M., Powell, R. M., Brenowitz, M. & Parkhurst, L. J. (2001). Bends in TATA-binding protein-TATA complexes in solution are DNA sequence-dependent. *J. Biol. Chem.*, 276 14614-14622.
38. Wu, J., Parkhurst, K. M., Powell, R. M. & Parkhurst, L. J. (2001). DNA sequence-dependent differences in TATA-binding protein-induced DNA bending in solution are highly sensitive to osmolytes. *J. Biol. Chem.* **276**, 14623-14627.
39. Birmachu, W., Nisswandt, F. L. & Thomas, D. D. (1989). Conformational transitions in the calcium adenosinetriphosphatase studied by time-resolved fluorescence resonance energy transfer. *Biochemistry*, **28**, 3940-3947.
40. Lillo, M. P., Beechem, J. M., Szpikowska, B. K., Sherman, M. A. & Mas, M. T. (1997). Design and characterization of a multisite fluorescence energy-transfer system for protein folding studies: a steady-state and time-resolved study of yeast phosphoglycerate kinase. *Biochemistry*, **36**, 11261-11272.
41. Warwicker, J., Engelman, B. P. & Steitz, T. A. (1987). Electrostatic calculations and model-building suggest that DNA bound to CAP is sharply bent. *Proteins: Struct. Funct. Genet.* **2**, 283-289.
42. Dalma-Weiszhausz, D. D., Gartenberg, M. R. & Crothers, D. M. (1991). Sequence-dependent contribution of distal binding domains to CAP protein-DNA binding affinity. *Nucl. Acids Res.* **19**, 611-616.
43. Grinvald, A., Haas, E. & Steinberg, I. Z. (1972). Evaluation of the distribution of distances between energy donors and acceptors by fluorescence decay. *Proc. Natl Acad. Sci. USA*, **69**, 2273-2277.
44. James, D. R., Turnbull, J. R., Wagner, B. D., Ware, W. R. & Petersen, N. O. (1987). Distributions of fluorescence decay times for parinaric acids in phospholipid membranes. *Biochemistry*, **26**, 6272-6277.
45. Johnson, I. D. & Hudson, B. S. (1989). Environmental modulation of M13 coat protein tryptophan fluorescence dynamics. *Biochemistry*, **28**, 6392-6400.
46. Selvin, P. R. & Hearst, J. E. (1994). Luminescent energy transfer using a terbium chelate: improvements on fluorescence energy transfer. *Proc. Natl Acad. Sci. USA*, **91**, 10024-10028.
47. Heyduk, E. & Heyduk, T. (1997). Thiol-reactive, luminescent europium chelates: luminescent probes for resonance energy transfer distance measurements in biomolecules. *Anal. Biochem.* **248**, 216-227.
48. Berendsen, H. J. & Hayward, S. (2000). Collective protein dynamics in relation to function. *Curr. Opin. Struct. Biol.* **10**, 165-169.
49. Cheatham, T. E., III. & Kollman, P. A. (2000). Molecular dynamics simulation of nucleic acids. *Annu. Rev. Phys. Chem.* **51**, 435-471.
50. Stryer, L., Thomas, D. D. & Meares, C. F. (1982). Diffusion-enhanced fluorescence energy transfer. *Annu. Rev. Biophys. Bioeng.* **11**, 203-222.
51. Callaci, S., Heyduk, E. & Heyduk, T. (1999). Core RNA polymerase from *E. coli* induces a major change in the domain arrangement of the sigma70 subunit. *Mol. Cell*, **3**, 229-238.
52. Heyduk, T., Lee, J. C., Ebright, Y. W., Blatter, E. E., Zhou, Y. & Ebright, R. H. (1993). CAP interacts with RNA polymerase in solution in the absence of promoter DNA. *Nature*, **364**, 548-549.
53. Ozaki, H. & McLaughlin, L. W. (1992). The estimation of distances between specific backbone-labelled sites in DNA using fluorescence resonance energy transfer. *Nucl. Acids Res.* **20**, 5205-5214.
54. Zhou, Y. H., Zhang, X. P. & Ebright, R. H. (1991). Random mutagenesis of gene-sized DNA molecules by use of PCR with *Taq* DNA polymerase. *Nucl. Acids Res.* **19**, 6052.
55. Kunkel, T., Bebenek, K. & McClary, J. (1991). Efficient site-directed mutagenesis using uracil-containing DNA. *Methods Enzymol.* **204**, 125-138.
56. Miller, J. (1972). *Experiments in Molecular Genetics*, Cold Spring Harbor Laboratory Press, Cold Spring Harbor, NY.
57. Zhang, X. P., Gunasekera, A., Ebright, Y. W. & Ebright, R. H. (1991). Derivatives of CAP having no solvent-accessible cysteine residues, or having a unique solvent-accessible cysteine residue at amino acid 2 of the helix-turn-helix motif. *J. Biomol. Struct. Dyn.* **9**, 463-473.
58. James, D. R., Siemiarczuk, A. & Ware, W. R. (1992). Stroboscopic optical boxcar technique for the determination of fluorescence lifetimes. *Rev. Sci. Instr.* **53**, 1710-1716.
59. Lakowicz, J. R. (1986). A review of photon-counting and phase-modulation measurements of fluorescence decay kinetics. In *Application of Fluorescence in the Biomedical Sciences* (Taylor, D. L., ed.), pp. 29-67, Alan R. Liss Inc., New York.
60. Chen, R. F. & Bowman, R. L. (1965). Fluorescence polarization: measurement with ultraviolet-polarizing filters in a spectrofluorometer. *Science*, **147**, 729-732.

61. Hudson, E. & Weber, G. (1973). Synthesis and characterization of two fluorescent sulfhydryl reagents. *Biochemistry*, **12**, 4154-4161.
62. Cross, A. J. & Fleming, G. R. (1984). Analysis of time-resolved fluorescence anisotropy decays. *Biophys. J.* **46**, 45-56.
63. Kinoshita, K., Jr., Kawato, S. & Ikegami, A. (1977). A theory of fluorescence polarization decay in membranes. *Biophys. J.* **20**, 289-305.
64. Dale, R. E., Eisinger, J. & Blumberg, W. E. (1979). The orientational freedom of molecular probes. *Biophys. J.* **26**, 161-194.
65. Haas, E., Katchalski-Katzir, E. & Steinberg, I. Z. (1978). Effect of the orientation of donor and acceptor on the probability of energy transfer involving electronic transitions of mixed polarization. *Biochemistry*, **17**, 5064-5070.
66. Hagler, A. T., Osguthorpe, D. J., Dauber-Osguthorpe, P. & Hempel, J. C. (1985). Dynamics and conformational energetics of a peptide hormone: vasopressin. *Science*, **227**, 1309-1315.
67. Karplus, M. & Petsko, G. A. (1990). Molecular dynamics simulations in biology. *Nature*, **347**, 631-639.
68. Weiner, S. J., Kollman, P. A., Case, D. A., Singh, U. C., Ghio, C., Alagona, G. & Weiner, P. (1984). A new force field for molecular mechanical simulation of nucleic acids and proteins. *J. Am. Chem. Soc.* **106**, 765-784.
69. Andersen, H. C. (1983). RATTLE: a "velocity" version of the SHAKE algorithm for molecular dynamics calculations. *J. Comput. Phys.* **52**, 24-34.
70. Hagler, A. T., Stern, P. S., Sharon, R., Becker, J. M. & Naider, F. (1979). Computer simulation of the conformational properties of oligopeptides. Comparison of theoretical methods and analysis of experimental results. *J. Am. Chem. Soc.* **101**, 6842-6852.
71. Dauber-Osguthorpe, P., Roberts, V. A., Osguthorpe, D. J., Wolff, J., Genest, M. & Hagler, A. T. (1988). Structure and energetics of ligand binding to proteins: *Escherichia coli* dihydrofolate reductase-trimethoprim, a drug-receptor system. *Proteins: Struct. Funct. Genet.* **4**, 31-47.
72. Lim, K. & Herron, J. N. (1995). Molecular dynamics of the anti-fluorescein 4-4-20 antigen-binding fragment. 1. Computer simulations. *Biochemistry*, **34**, 6962-6974.
73. Verlet, L. (1967). Computer experiments on classical fluids. I. Thermodynamic properties of Lennard-Jones molecules. *Phys. Rev.* **159**, 98-103.
74. Ding, H. Q., Karasawa, N. & Goddard, W. A., III. (1992). Atomic level simulations on a million particles: the cell multipole method for Coulomb and London nonbond interactions. *J. Chem. Phys.* **97**, 4309-4315.
75. van der Heide, U. A., Orbons, B., Gerritsen, H. C. & Levine, Y. K. (1992). The orientation of transition moments of dye molecules used in fluorescence studies of muscle systems. *Eur. Biophys. J.* **21**, 263-272.
76. Xiao, M. & Selvin, P. (2000). Quantum efficiency of luminescent lanthanide chelates and far-red dyes measured by diffusion-enhanced energy transfer. *Biophys. J.* **78**, 129A.

Edited by P. E. Wright

(Received 21 May 2001; received in revised form 26 July 2001; accepted 1 August 2001)